Materials and Design 198 (2021) 109348

Contents lists available at ScienceDirect

Materials and Design

journal homepage: www.elsevier.com/locate/matdes

Impurity removal from Si by Si-Ca-Mg ternary alloying-leaching system

Mengyi Zhu [a,*], Di Wan [b,*], Kai Tang [c], Jafar Safarian [a]

[a] Department of Materials Science and Engineering, Norwegian University of Science and Technology, Trondheim, Norway
[b] Department of Mechanical and Industrial Engineering, Norwegian University of Science and Technology, Trondheim, Norway
[c] SINTEF Industry, Trondheim, Norway

HIGHLIGHTS

- Parametric study on the Si-Ca-Mg alloying-leaching system was carried out.
- Ca/Mg ratio and solidification conditions significantly affect microstructure.
- Leaching kinetics of Si-Ca-Mg alloy follows a modified Kröger-Ziegler model.
- Increasing Ca/Mg ratio promotes impurity removal.
- A model for P removal prediction was obtained for ternary Si alloy system.

GRAPHICAL ABSTRACT

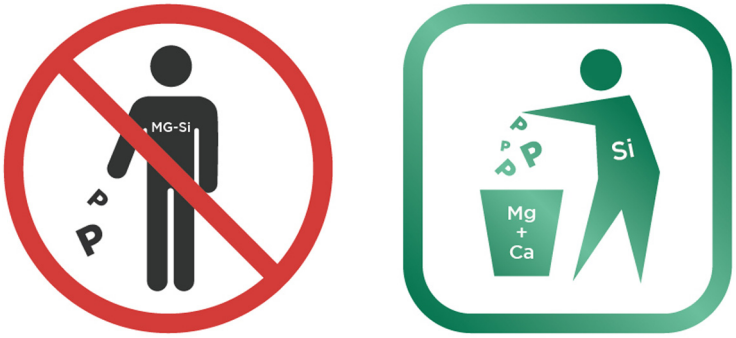

ARTICLE INFO

Article history:
Received 23 September 2020
Received in revised form 8 November 2020
Accepted 19 November 2020
Available online 21 November 2020

Keywords:
Silicon
Phosphorous
Impurity
Microstructure
Segregation
Thermodynamics

ABSTRACT

In this work, Si-Ca-Mg alloys were made with different compositions and solidification conditions to investigate the impurity segregation and separation performance from Si, especially for the crucial P impurity at several ppmw levels. Varying acid leaching parameters were also employed to investigate the optimized process window. Results indicate that the novel Si-Ca-Mg alloying-leaching system is valid for high P extraction. The ternary intermetallic phase $Ca_7Mg_{7.5\pm\delta}Si_{14}$ appears as the main precipitate in all alloys to gather other minor impurities. Rapid cooling significantly reduced the size of precipitates and Si grain, the impurity segregation was also limited. In the acid leaching experiments, HCl is found as the most economical leaching agents among the studied combinations. Smaller particle size promotes the leaching efficiency, but the increment narrows with increasing Ca/Mg ratio. Leaching kinetics of the studied alloys was found following the modified Kröger-Ziegler model based on a cracking-shrinking mechanism. The impurity purification efficiency increases with increasing Ca/Mg mixing ratio, but significantly reduced by rapid cooling. An analytical model was developed for ternary alloy system to predict the P segregation and its removal with varying alloy concentration through the thermodynamic approach, which shows good agreements of the experimental results.

1. Introduction

There is growing interest in developing a more environmentally friendly approach to produce solar-grade silicon (SoG-Si, purity 99.9999%) for the photovoltaic (PV) industry. The current SoG-Si production is dominated by the modified Siemens process and fluidized bed reactor process. As an emerging process with advantages of sustainability, the metallurgical route is known for lower energy consumption, lower carbon footprint, and less energy payback time [1–3]. Additionally, the increasing amount of the cutting kerf from Si ingot and the end-of-life Si solar panels has also made the metallurgical route become a potential candidate for the recycling of Si materials regarding a circular materials flow economy.

The main challenge for the metallurgical process is the removal of large amount of impurities from the metallurgical grade Si (MG-Si),

* Corresponding authors.
E-mail addresses: mengyi.zhu@ntnu.no (M. Zhu), di.wan@ntnu.no (D. Wan).

https://doi.org/10.1016/j.matdes.2020.109348

especially the problematic B and P impurities due to the restrict impurity concentration limits of SoG-Si. To date, a number of metallurgical processes have been studied for the purification of MG-Si to SoG-Si, including slag refining [4–10], solvent refining [11–15], acid leaching [16–18], vacuum refining [19–21], and gas refining [22–25]. Among the above purification techniques, acid leaching is known to play a crucial role in the removal of P impurity and other metallic impurities. The principle of acid leaching purification is to digest the impurity phase precipitated out of Si phase; however, in practice, the final purification efficiency is always affected by several processing factors. After the pioneering research performed by Tucker almost a century ago [26] for the MG-Si leaching, extensive interest in Si purification has been paid afterward to seek the optimal purification conditions [27–31]. Kim et al. [32] studied the dissolution window of Fe silicides and found the leaching efficiency is dependent on the acid combination and impurity phase composition. The reactivity of impurity precipitates was determined by Margarido et al. [33,34] and the leaching kinetics of ferrosilicon were found to follow a cracking-shrinking core model [35]. Recently, several alloying elements were introduced into MG-Si as impurity getter to modify the impurity precipitation and further enhance the leaching efficiency. One successful approach is known as the solvent refining, which aims at low-temperature operation by adding large amounts of alloying elements such as the well-studied Si-Al [36–41], Si-Cu [12,42], and Si-Fe [43–45] systems. Another alloying approach is adding only a limited amount of additives but with strong impurity affinity as an impurity getter. Ca [17,46–49] is the most often studied alloying impurity getter due to its strong affinity to P to form the stable compound Ca_3P_2. In the recent study from our group [16,50–52], Mg also exhibited high P affinity in Si and the effectiveness of large extent impurities extraction. The separation of the alloy phase by hydrometallurgical treatment was found affected by a variety of leaching parameters such as temperature, acid combination, particle size, and alloying concentration.

The ternary Si-Ca-Mg system is a novel alloying-leaching refining system with different alloying phases. Subsequently, the leaching behavior differs with the binary Si-Ca and Si-Mg system. However, there is still a lack of understanding and investment in the ternary system. Thus, in the present work, a parametric study is carried out to investigate the ternary Si-Ca-Mg system aiming to reveal the effect of a number of factors on the final impurity separation performance. Alloys with different compositions were prepared and refined under different conditions. The effect of Ca/Mg mixing ratio and cooling rate on the microstructural evolution, purification efficiency, and Si recovery were examined and compared as well as the impact of different leaching agents and particle sizes on the impurity removal efficiency. The leaching kinetics was also investigated based on a developed cracking-shrinking model. Finally, a purification model for P removal was established for the ternary alloy system through a thermodynamic approach and Gulliver-Scheil solidification principles.

2. Experimental

2.1. Sample preparation

Commercial MG-Si was used as the starting Si source and physically mixed with a specific amount of impurity-free fluidized bed Si (FBR-Si) to attain the P impurity (as the main element of interest) as low as several ppmw levels. High purity Mg (99.8% purity, Alfa Aesar) and granular Ca (99% purity, Sigma Aldrich) were selected as the doping metal materials. As shown in Fig. 1, the composition of selected alloys was initially designed to obtain different Ca/Mg mixing mole ratios as Ca/Mg = 0.5 (1.5 mol% Ca and 3.0 mol% Mg), 1 (2.25 mol% Ca and 2.25 mol% Mg), and 2 (3.0 mol% Ca and 1.5 mol% Mg), respectively, which are marked as CM0.5, CM1, and CM2 in this work. In addition, a casted alloy (marked as CM1-Casted) with the composition closes to sample CM1 was also made to study the cooling rate effect. It is also

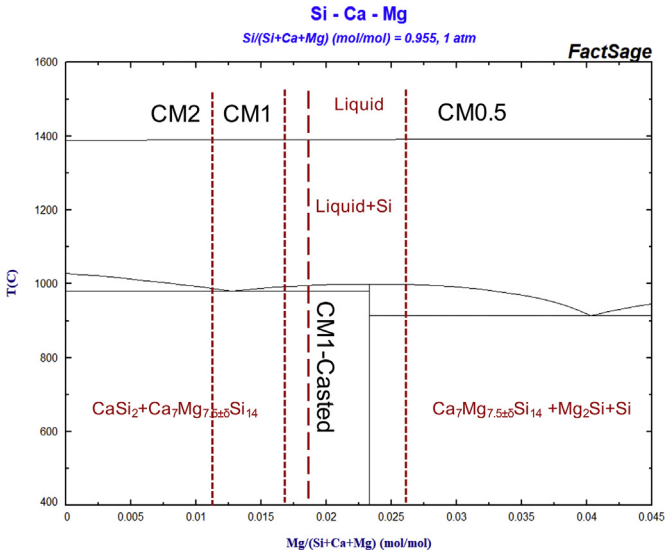

Fig. 1. Phase diagram of Si-Ca-Mg system with the designed sample composition, calculated by FactSage®. (digital version in color).

worth noting that as the alkaline-earth metals evaporate at the high-temperature, the final obtained alloy composition will be slightly different but close to the Ca/Mg ratio as designed. Prior to the alloy melting process, around 400 g Si mixtures (160 g MG-Si and 240 g FBR-Si) were put into a high-density graphite crucible with a specific amount of Ca addition, while Mg piece was doped later after melting, respectively, 9.2 g Ca and 11.5 g Mg for CM0.5, 13.8 g Ca and 8.3 g Mg for CM1, 18.4 g Ca and 5.6 g Mg for CM2, and 13.3 g Ca and 8.1 g Mg for CM1-Casted. The graphite crucible was then heated in an induction furnace under a pure Ar (99.9999% purity) flow atmosphere. The molten alloy was held at 1773 K for 10 min with intensive stirring flow induced by the induction heating and yielded proper melt homogenization. The melt was then slowly cool down in the furnace (cooling rate c.a. 10^{-1}–10^{1} K/s) or cast to a water-cooled copper mold (cooling rate 10^{2}–10^{3} K/s). The obtained Si-Ca-Mg bulk alloys were then crushed and milled in a ring mill to the target particle sizes (0.2–1 mm and < 0.2 mm) using Retsch Vibratory Disc Mill RS200 with the tungsten carbide sets. The final compositions of the alloys determined by a high resolution inductively coupled plasma mass spectroscopy (ICP-MS, Agilent 8800) after sizing are listed in Table 1.

Table 1
Measured compositions of MG-Si and obtained Si alloys (ppmw).

Sample	Particle size (mm)	P	Ca	Mg	Al	Fe	Ti	Zr
MG-Si	Lump	14.8	331.7	10.7	1859.7	2723.9	218.2	7.9
CM0.5	0.2–1	4.5	14,780.1	21,533.3	539.7	783.9	68.8	3.0
	<0.2	7.1	27,658.0	39,360.4	936.6	1397.2	122.0	4.7
	Master alloy	5.2	18,173.4	26,230.7	644.3	945.5	82.9	3.4
CM1	0.2–1	4.7	23,182.8	13,884.1	565.6	805.2	71.2	2.8
	<0.2	6.4	38,940.6	23,163.2	910.3	1277.2	116.7	5.9
	Master alloy	5.3	27,910.1	16,667.8	669.0	946.8	84.9	3.7
CM2	0.2–1	4.3	27,668.0	8981.9	510.9	746.8	66.9	5.1
	<0.2	5.9	51,559.8	15,961.7	881.1	1325.8	117.5	4.1
	Master alloy	4.7	34,092.5	10,858.8	610.4	902.5	80.5	4.8
CM1-Casted	0.2–1	4.8	22,040.0	15,696.6	635.6	917.8	90.6	3.2
	<0.2	6.1	26,938.6	19,629.6	781.8	1201.0	113.3	4.0
	Master alloy	5.1	23,416.5	16,801.8	676.7	997.4	97.0	3.4

2.2. Characterization

Metallographic samples were prepared for the microstructural characterization. Electron Probe Micro-Analyzer (EPMA, JXA-8500F) supported with wavelength-dispersive spectroscopy (WDS) was applied for the elemental mapping and phase composition determination. The crystallographic properties were also measured by electron backscattered diffraction (EBSD) using NORDIF system. The EBSD scan was conducted in a Quanta 650 scanning electron microscope (SEM, ThermoFisher Scientific Inc.) operated at an accelerating voltage of 20 kV, an aperture of 100 μm and a spot size of 4.0. The working distance was about 20 mm for the 70° pre-tilt specimen, and the dynamic focus in the SEM was adopted to improve the focal distance over a relatively large probe area of about 1.2×1.2 mm^2.

2.3. Leaching-refining trials

Acid leaching experiments for the impurity segregation and removal study were carried out by mixing 2 g samples and 10 mL 10% HCl solutions in perfluoroalkoxy alkane (PFA) bottles, which were in a bath with ultrasonic-assisted mixing. The leaching conditions are determined according to our previous investigations [53] that the leaching temperature was set at 60 °C with a leaching period of 0–3 h. Several leaching agent combinations were designed to compare the leaching efficiency using CM0.5 (particle size 0.2–1 mm) as a reference sample, including HCl, concentrated aqua regia, diluted aqua regia (50%), HCl + 10% $FeCl_3$ (volume ratio), HCl + 10% Glycerin, and HCl + 10% oxalic acid ($C_2H_2O_4$). The leached samples were then washed by deionized water and ethanol. The impurity concentrations in all samples were measured by high-resolution ICP-MS as the alloys.

3. Results and discussion

The obtained results are presented and discussed with supplementary theoretical calculations as follows.

3.1. Microstructure

3.1.1. Effect of Ca/Mg mixing ratio

The effect of the Ca/Mg mixing ratio on the alloy microstructure and the segregation of metallic impurities such as Ca, Mg, Al, Fe, and Ti, were characterized by EPMA elemental mapping. As the results presented in Fig. 2, impurities are found concentrated in the regions at the end stage of solidification. It is also seen that the alloy microstructure is significantly affected by the alloy composition as the large phases are marked in the backscattered electrons (BSE) image. The ternary intermetallic $Ca_7Mg_{7.5\pm\delta}Si_{14}$ phase is found as the common main precipitate that appears in all the Si-Ca-Mg alloys. The binary precipitate Mg_2Si and $CaSi_2$ are also found coexist with $Ca_7Mg_{7.5\pm\delta}Si_{14}$, respectively, in samples CM0.5 and CM2, as the phase diagram suggested in Fig. 1. However, it is worth noting that in sample CM1, the precipitates Mg_2Si, $Ca_7Mg_{7.5\pm\delta}Si_{14}$, and $CaSi_2$ are observed together, which is not thermodynamically preferred. This may be related to non-equilibrium solidification even when the samples are cooled down in the furnace. Unlike the microstructure observed in binary Si-Ca and Si-Mg alloys, in the Si-Ca-Mg alloying system, Al is found most likely to be dissolved in the ternary $Ca_7Mg_{7.5\pm\delta}Si_{14}$ phase as the form of the solid solution rather than to form specific compounds. Transition-metal silicide is an essential family of the intermetallic phases in MG-Si, also known with poor reactivities to acids. Iron is the most abundant impurity in MG-Si and distributed as single secondary precipitate phase in the Si matrix. However, in all of the obtained Si-Ca-Mg alloys, Fe impurity is found only located inside the $Ca_7Mg_{7.5\pm\delta}Si_{14}$ phase with fine Ti impurity particles being adjacent. The result of EPMA-WDS point analysis further indicates the Fe-bearing phase is with the stoichiometry Fe_3Si_7, which is in agreement with the high-temperature $FeSi_2$ phase (also known as $FeSi_{2.4}$ or α-leboite) that stabilized by Al impurity down to room temperature [54,55]. However, a certain extent ultrafine low-temperature $FeSi_2$ phase with Si could also possibly exist as the decompose products of the high-temperature stable Fe_3Si_7 phase but cannot be fully separated and detected due to the slow solid-solid decompose reaction. Thus, in the present work, the Fe-bearing phase is described as $Fe_3Si_7(FeSi_2 + Si)$. Since the transition metal impurity phases are gathered in the leachable ternary $Ca_7Mg_{7.5\pm\delta}Si_{14}$ phase, it may also imply the effectiveness of enhanced Fe and Ti removal with Ca and Mg alloying.

3.1.2. Effect of cooling rate

The microstructure of MG-Si and Si alloys is greatly affected by the solidification condition [47,56]. As presented in Fig. 3, the typical precipitates of the CM1-Casted sample were also characterized by EPMA elemental mapping, which is observed still as $Ca_7Mg_{7.5\pm\delta}Si_{14}$, $CaSi_2$, and $Fe_3Si_7(FeSi_2 + Si)$, but all with a much less and fine structure. In addition, it is also seen that a large fraction of Si islands embedded inside the main precipitates.

The elemental composition of each precipitate is also imperative to compare since it may imply the segregation extent information of impurities. Thus, the detected atomic fraction of each phase in sample CM1 and CM1-Casted were analyzed by EPMA, as listed in Table 2. By comparing the purity of the Si matrix, it is found that the Si matrix in the sample CM1-Casted contains more impurities since the Si purity 99.60% is slightly lower than that of the sample CM1 with the Si purity 99.76%. Furthermore, the measured composition of all precipitates shows a higher Mg concentration in the sample CM1-Casted. Even though the considerably high Mg atomic fraction (7.01%) in the $Fe_3Si_7(FeSi_2 + Si)$ phase may be owing to the measuring error caused by the thin precipitate thickness, the higher Mg/Ca ratio also suggests the findings. Another evidence for the limited impurity segregation via fast cooling can be obtained from the measured composition of different particle sizes listed in Table 1. For instance, the composition differences of CM1-Casted with different particle sizes are narrower than that of the other three furnace cooled samples, demonstrating a more homogenized and less segregated impurity distribution. Thus, it is concluded that the fast cooling of the Si-Ca-Mg alloys leads to insufficient segregation of impurities and the non-equilibrium precipitation at the end of solidification.

The comparison of the microstructure between the furnace cooled sample CM1 and casted sample CM1-Casted can be seen in Fig. 4. By comparing the overview images shown in Fig. 4(a) and Fig. 4(c), apparently, it is found that the precipitates in the sample CM1 are much less and coarser than that of the sample CM1-Casted. Meanwhile, in the sample CM1-Casted, the size of the precipitates and Si both shrink dramatically.

Since the crystal structural parameters may directly reflect the properties of the material, EBSD measurement was applied to further investigate the effect of cooling rate on the Si grain structural properties. As presented by Fig. 4(b) and Fig. 4(d), it can be seen that the Si grains in the furnace cooled sample CM1 are much larger than that of the casted sample CM1-Casted, and most of the precipitated phases (the dark areas) are also found located along the Si grain boundary. Thus, most of the precipitates would be exposed after crushing, and the Si grains would remain after leaching. However, practically, the final Si recovery could be reduced by the fast cooling as the fine Si grains (especially the ultrafine Si grains shown in Fig. 4(b)) could increase Si loss during the leaching and the post Si-collecting process.

The corresponding crystallographic orientation (in terms of normal direction of the sample) is also captured by different colors. It is observed that CM1-Casted sample shows more random and messy crystal orientation distribution, which reflects the profoundly disturbed primary Si crystal growth condition by casting. Consequently, the impurity segregation is limited and more impurities could be trapped by the growing Si crystal so that further limits the final purification performance according to the mechanism proposed by Ban et al. [57]. Thus, even with similar alloy compositions, the Si purification efficiency could be significantly affected by the solidification conditions.

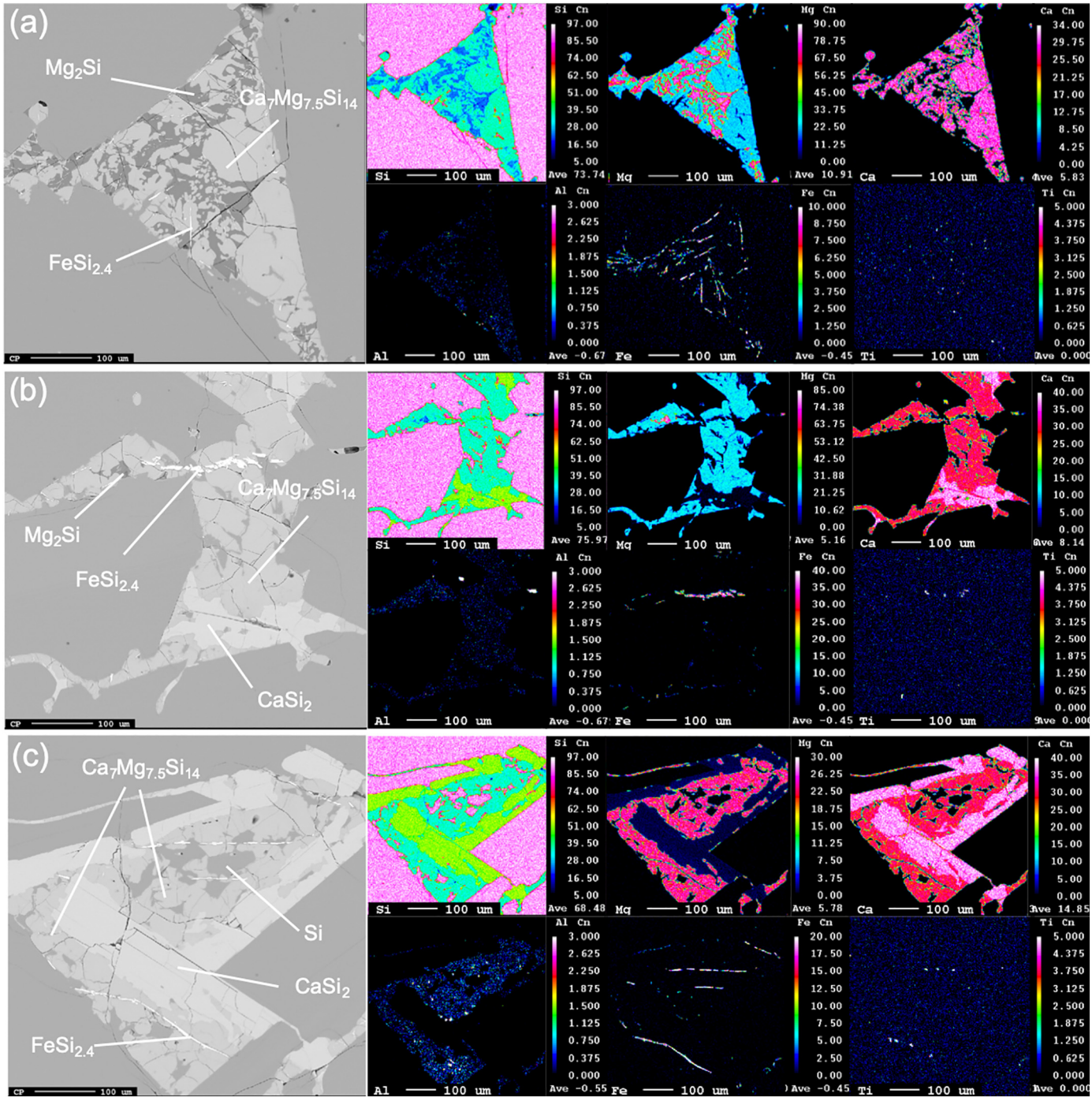

Fig. 2. Typical precipitates and EPMA elemental mapping results of studied alloys (a) sample CM0.5, (b) sample CM1, and (c) sample CM2. (digital version in color).

3.2. Leaching characteristics

In this section, a variety of leaching parameters and characteristics are discussed, including the effect of leaching agents, particle size, and leaching kinetics. It is worth noting that the leaching efficiency is defined here as the percentage of extracted impurity of the initially charged materials (coarse or fine particles) listed below:

$$\text{Leaching efficiency} = \frac{C_{\text{particles for leaching}} - C_{\text{after leaching}}}{C_{\text{particles for leaching}}} \times 100\% \quad (1)$$

where the $C_{\text{particles for leaching}}$ and $C_{\text{after leaching}}$ are initial impurity concentration of coarse or fine Si alloy particles and the final impurity concentration of leached Si in weight percent, respectively.

3.2.1. Effect of leaching agents

After obtaining knowledge of the microstructure of the Si-Ca-Mg alloys, it is then necessary to determine the suitable leaching agents. On the basis of our previous work [50], HCl (10%) aqueous solution was found the most effective compared to other commonly used acids. Accordingly, several HCl-based leaching combinations and aqua regia solutions were employed to study their effect on the leaching efficiency as the results shown in Fig. 5. It is also worth to noting that the comparison is only restricted to the acid solution with the selected concentration. It is seen that almost all of the doped Ca and Mg can be removed by the selected acid combinations, only the combination of HCl + 10% Glycerin shows a slightly lower efficiency as 93% removal and the highest efficiency 97% is achieved by the diluted aqua regia and HCl + 10% $FeCl_3$. Meanwhile, HCl + 10% $FeCl_3$ is also found the most

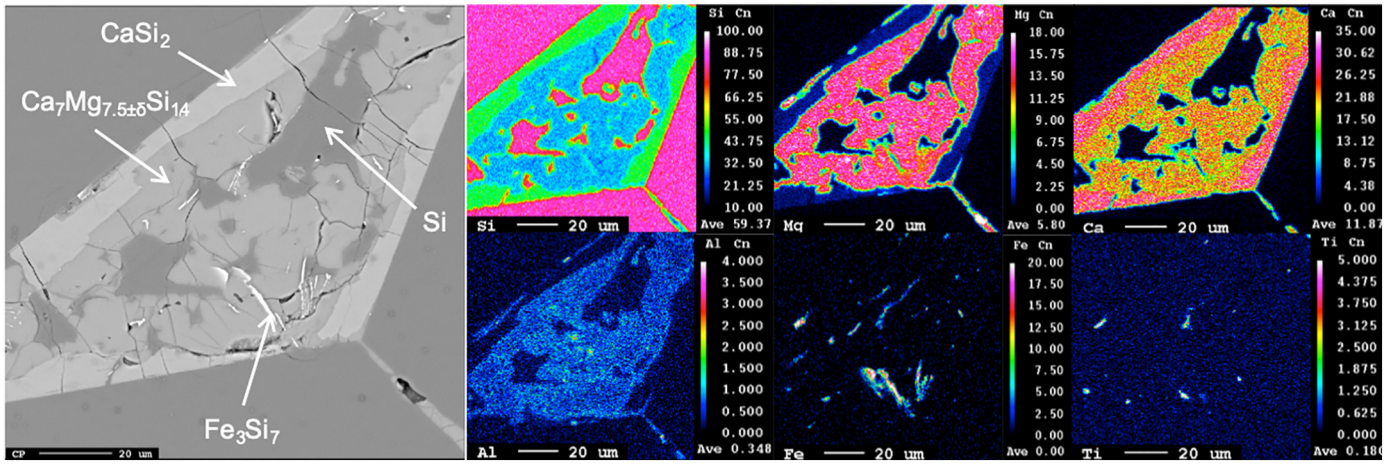

Fig. 3. EPMA elemental mapping results of sample CM1-Casted. (digital version in color).

Table 2
Detected composition (in at.%) of phases in sample CM1 and CM1-Casted by EPMA.

Sample	Phase	Si	Mg	Ca	Al	Fe
CM1	Si	99.76	0.10	0.11	0.03	0.01
	$CaSi_2$	66.59	1.59	31.71	0.11	0.01
	$Ca_7Mg_{7.5}Si_{14}$	48.77	25.94	24.42	0.85	0.01
	Fe_3Si_7($FeSi_2$ + Si)	68.89	0.81	0.82	0.53	28.95
CM1-Casted	Si	99.60	0.23	0.12	0.05	0.01
	$CaSi_2$	65.77	2.79	31.33	0.10	0.01
	$Ca_7Mg_{7.5}Si_{14}$	47.03	28.98	22.99	0.99	0.01
	Fe_3Si_7($FeSi_2$ + Si)	66.21	7.01	4.10	0.68	22.00

effective for the Al extraction that 79% removal is obtained. However, for the extraction of the transition metals impurities, concentrated aqua regia and its diluted solutions appear to be inefficient as leaching efficiency is only around 30–40%, while the addition of $FeCl_3$, Glycerin, and oxalic acid all reached the leaching efficiency around 50%. The reason may be owing to the strong oxidizing environment caused by the aqua regia so that the Si anion in the silicide phase is likely to be oxidized to SiO_2, subsequently, hinders the leaching kinetics, which is also suggested by Kim et al. [58] by the phase stability analysis. On the contrary, as the addition of $FeCl_3$ accelerates the particle disintegration [33], it then results in a faster kinetics. Thus, the combination of HCl + 10% $FeCl_3$ is seen with the highest leaching efficiency overall. Nevertheless, it is seen that HCl aqueous solution without additives also exhibits satisfying leaching results at a cheaper cost. In summary, the reactivity of acids for interacting with the studied Si-Ca-Mg alloy can be ordered as:

HCl + 10% $FeCl_3$ > HCl > HCl + 10% $C_2H_2O_4$ ≈ HCl + 10% Glycerin > Diluted aqua regia (50%) > Aqua regia.

3.2.2. Effect of particle size

Leaching efficiency is sensitive to the silicon particle size, and generally, higher efficiency is obtained by decreasing the particle size. The reason is attributed to the more exposed surface to acid solution by particle size reduction. In this work, two different particle sizes (coarse particle with range 0.2–1 mm and fine particle with diameter < 0.2 mm) were treated in HCl (10%) aqueous solution for 1 h at 60°C. As the results presented in Fig. 6, the leaching efficiency of most of the impurities is higher with fine particle size, especially for the sample CM0.5. For instance, the efficiency of Ca and Mg extraction increased from 95% to 99%, the Al extraction increased from 74% to 84%, and both of the Fe and Ti leaching efficiency improved from around 45% to 54% as well. However, it is seen that the increment of CM1 and CM2 turns into smaller by the fine particles leaching. Comparatively, the leaching efficiency of Ca, Mg, and Al of sample CM2 with different particle sizes are almost equivalent, and only the extraction of Fe and Ti have been increased from 62% to 70%, and from 65% to 71%, respectively. The increment of Ca, Mg, and Al of sample CM1 are seen in between sample CM0.5 and CM2, while the abnormal equivalent extraction of Fe and Ti impurities with different particle sizes is more likely deviations from slightly uneven sampling. The reason for the smaller leaching efficiency enhancement of increasing Ca/Mg ratio by the particle size reduction is considered owing to the strong cracking tendency of the $CaSi_2$ phase during leaching. As a result, the coarse particle disintegrates into the finer particle itself so that the leaching kinetics is being improved spontaneously. Thus, our result may also highlight the fact that the reduction of particle size could become unimportant for the leaching of the Si alloys contains the main phase with fast leaching kinetics. This is because, like dealing with Si-Ca-Mg alloys with high Ca content, the strong cracking effect could "auto-catalyze" the leaching process itself. In addition, in practice, the enhancement of leaching efficiency through particle size reduction might also be not significant enough to compensate for the cost of the extra process and more material losses.

3.2.3. Leaching kinetics

The leaching kinetics of Si-Ca-Mg alloys was investigated by performing a series of leaching trials of sample CM0.5 in different leaching periods of 5, 10, 20, 30, 45, 60 and 120 min by HCl (10%) at 60 °C under ultrasonic bath within the particle size range 0.2–1 mm. The results of the impurity extraction degree against leaching time are plotted in Fig. 7(a). It is seen that most of the impurity extraction took place in the first one hour, especially at the initial stage. After 20 min leaching, 88.2% of Ca and Mg, 67.2% of Al, 50.2% of P, and around 40% of Fe and Ti were extracted. In addition, it is also seen that impurities can be classified into three groups from the leaching time plot and follows kinetics trend: Ca, Mg > Al, P > Ti, Fe. Apparently, as the main phase and the impurity getter, Ca and Mg exhibit the fastest kinetics. The similar extraction trend of Al and P may suggest that P could also distribute in the ternary $Ca_7Mg_{7.5\pm\delta}Si_{14}$ phase, as the EPMA elemental mapping results of Al shown in Fig. 2. The impurity extraction curve also reveals that Ti impurity stays together with Fe as suggested by the EMPA mapping results shown in Fig. 2 as well.

Martins and Magarido [59] developed a cracking-shrinking core model for the leaching of Si-Fe alloy system since the acid leaching of Si-based alloys are often found with cracking effect [33]. However, for the leaching of Si-Ca-Mg alloys in this work, this model failed to fit out results linearly. Nevertheless, a novel cracking-shrinking based model is found valid for the Si-Ca-Mg alloy system by employing the cracking

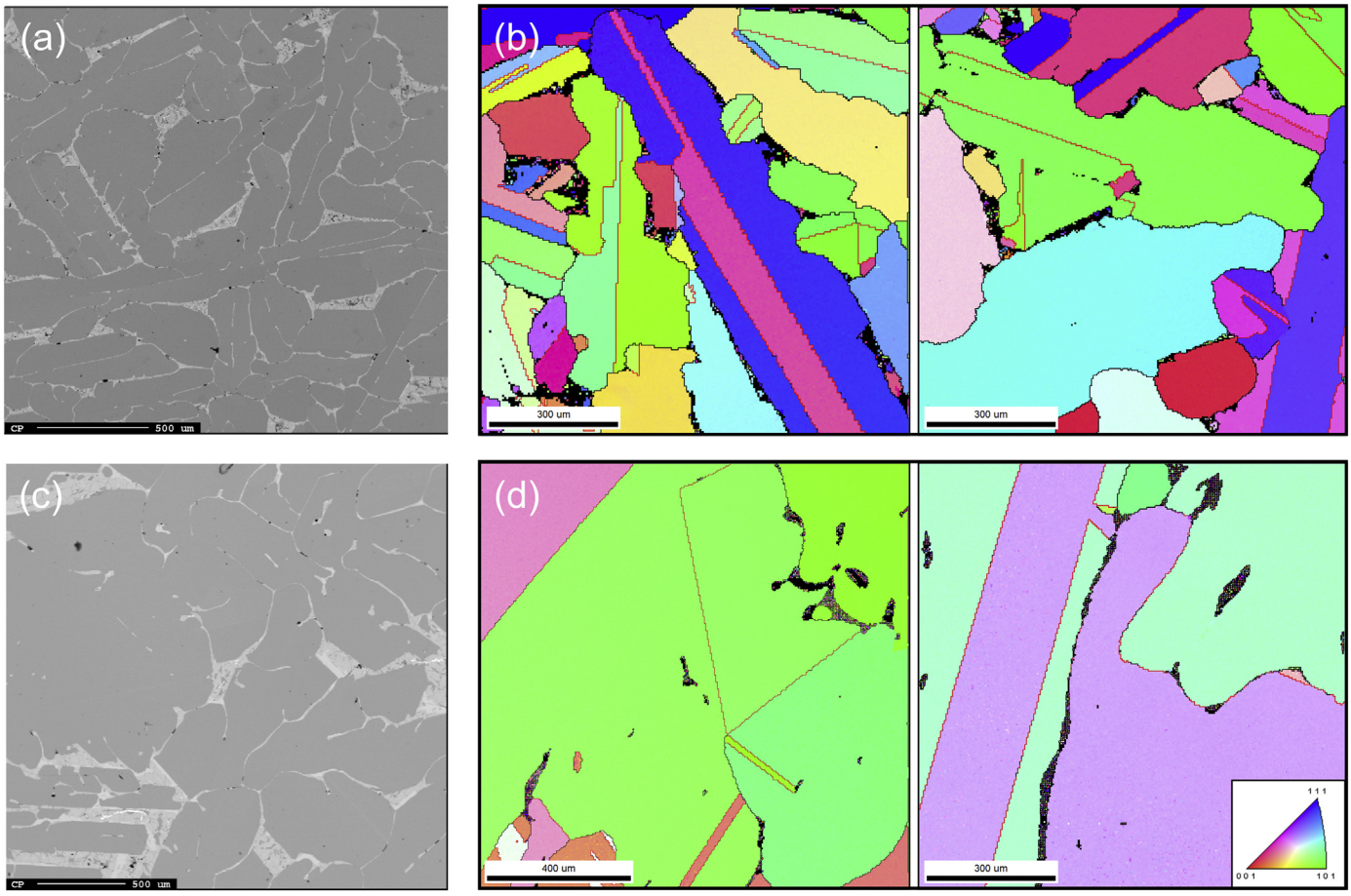

Fig. 4. Effect of cooling rate on Si-Ca-Mg alloy microstructure. (a) BSE image of sample CM1-Casted (b) EBSD crystallographic mapping of CM1-Casted (c) BSE image of sample CM1 (d) EBSD mapping of sample CM1. For EBSD maps: orientation with respect to the normal direction of the sample, color-coded according to the legend in the bottom-right corner. Black lines indicate high-angle grain boundaries (misorientation >15°) and red lines indicate twin boundaries. (digital version in color).

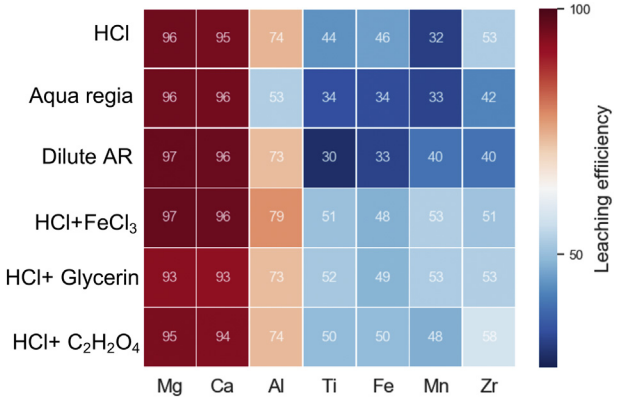

Fig. 5. The effect of leaching agents on the impurities removal (%) from sample CM0.5, leached at 60 °C with particle size of 0.2–1 mm. (digital version in color).

feature to a modified Kröger-Ziegler model with the consideration of spherical shrinking condition.[52] It is assumed that particle surface was first attacked by acids during the leaching. With the propagation of the surface micro-cracks, the whole particle eventually disintegrates at the time t_c with the impurity conversion X_c. For simplification, only one-time particle disintegration assumed to happen. Thus, a core shrinking stage is considered to start with $t \geq t_c$ and the impurity conversion is re-normalized as $\alpha = \frac{X-X_C}{1-X_C}$. Thus, the kinetic relationship is described as two stages, respectively:

Cracking stage:

$$X = k_C t \ (0 \leq t < t_c) \ (2)$$

Shrinking stage:

$$1-\frac{2}{3}\left(\frac{X-X_C}{1-X_C}\right)-\left(1-\left(\frac{X-X_C}{1-X_C}\right)\right)^{\frac{2}{3}} = K_S \ln\left(\frac{t}{t_c}\right) \ (t_c \leq t) \ (3)$$

where k_C and k_S are the rate constant of the cracking stage and the K-Z model. Additionally, since the conversion of Ca and Mg is always synchronous and the fastest in the leaching of Si-Ca-Mg alloy, the conversion of impurity i after cracking can be expressed as $X_{i,\,c} = \xi_i X_c^{Mg+Ca}$, where $\xi_i \in [0,1]$ and indicates the relative reaction rate of impurity i compared to Ca and Mg. Thus, the cracking-shrinking model is also written as:

$$Y(X_i) = 1-\frac{2}{3}\left(\frac{X_i-\xi_i X_c^{Mg+Ca}}{1-\xi_i X_c^{Mg+Ca}}\right)-\left(1-\left(\frac{X_i-\xi_i X_c^{Mg+Ca}}{1-\xi_i X_c^{Mg+Ca}}\right)\right)^{\frac{2}{3}} = K_S \ln\left(\frac{t}{t_c}\right) \ (t \geq t_c) \ (4)$$

It is also worth noting that special treatment needs to be paid to the P fitting because not all the P had chance to participate in the reaction as

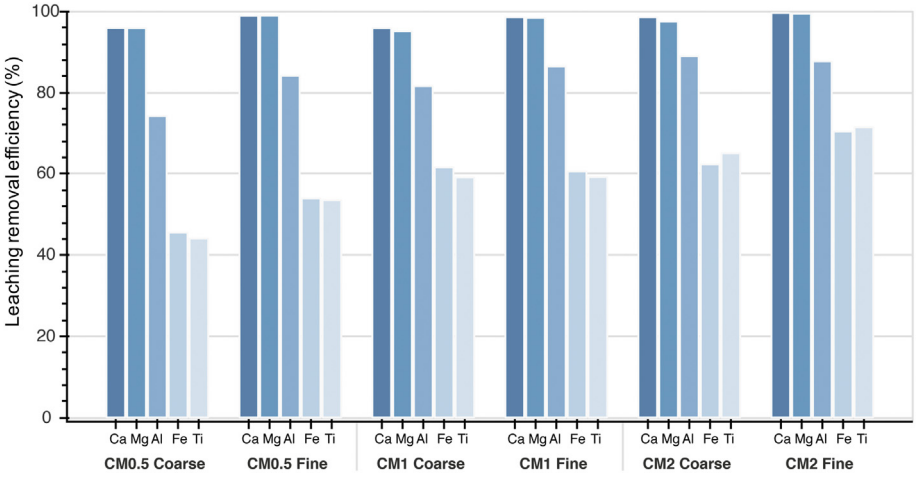

Fig. 6. Effect of particle size on the leaching efficiency by 10% HCl for "Coarse", and "Fine" alloy samples. (digital version in color).

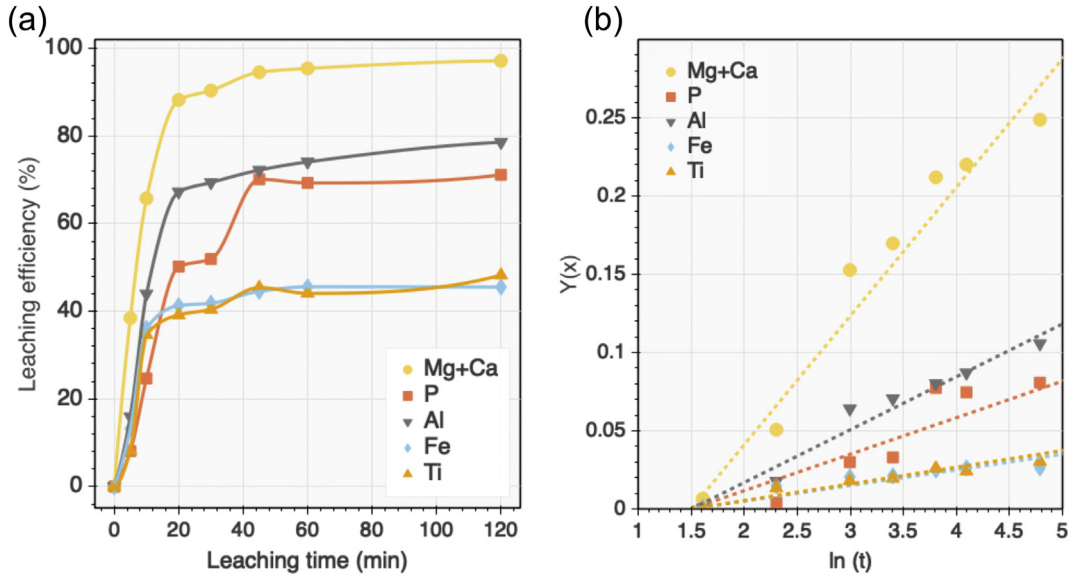

Fig. 7. Effect of leaching time on impurity removal of sample CM0.5 (0.2–1 mm particles by HCl at 60 °C) (b) Application of the cracking-shrinking model to studied impurities Mg + Ca, P, Al, Fe, and Ti. (digital version in color).

only the part of P segregated outside the Si primary grains is leachable, and the rest is dissolved in the structure of Si matrix. Consequently, the effective P conversion is introduced as:

$$X_{P,eff} = \frac{\eta N_{total} - N_t}{\eta N_{total}} \quad (5)$$

where N_{total} and N_t denote the overall P concentration and the P concentration with leaching time t. η is the percentage that P segregated into precipitates, which is estimated as 0.85 from the final leaching purification results.

By fitting the data of the leaching results, linear relationship was observed between $Y(X_i)$ and ln t as shown in Fig. 7(b). Meanwhile, one of the main features is seen is that all fitting lines origins from the starting point, which indicates the assumed cracking time. The relevant fitting parameters and obtained rate constants are listed in.

Table 3. The results demonstrate that the leaching cracking stage occurs in a short time which indicates the intensive reaction happened at the beginning of leaching. In addition, impurity extraction kinetics follows the order as discussed above that: Ca, Mg > Al > P > Ti ≈ Fe.

3.3. Purification efficiency

The purification efficiency of studied alloys (CM0.5, CM1, CM2, and CM1-Casted) and MG-Si after leaching under the same conditions that with HCl (10%) at 60 °C under ultrasonic bath for the particle size ranges from 0.2 to 1 mm. The purification efficiency is calculated as:

Table 3
The obtained kinetic parameters from cracking-shrinking model for the impurities extraction from sample CM0.5.

Impurity	$ln(t_c)$ (min)	Xc 1	ξ 1	K_C (min^{-1})	K_S 1
Mg + Ca	1.5	0.2	1.0	0.045	0.082
P			0.4	0.018	0.022
Al			0.6	0.027	0.034
Fe			0.2	0.009	0.011
Ti			0.2	0.009	0.011

$$Purificationefficiency = \frac{C_{bulkmaterial} - C_{afterleaching}}{C_{bulkmaterial}} \times 100\% \quad (6)$$

where $C_{bulk\ material}$ represents the initial impurity concentration of the bulk Si master alloy or MG-Si, and $C_{after\ leaching}$ is the final impurity concentration of leached Si in weight percent.

The compositions of purified Si are listed in Table 4 and the calculated purification efficiency results are compared in Fig. 8. A distinct trend can be seen that the purification efficiency for all impurities follows the order: MG-Si < CM1-Casted< CM0.5 < CM1 < CM2. Hence, it is concluded that the Ca—Mg alloying significantly improves the impurity removal and the purification efficiency increases with increasing Ca/Mg ratio and decreases with increasing cooling rate. Taking into account the P extraction, the purification efficiency is, respectively, 31.7% (MG-Si), 62.2% (CM1-Casted), 81.1% (CM0.5), 83.1% (CM1), and 87.0% (CM2).

The variation of the purification efficiency for each impurity is related to the impurity segregation behavior affected by the doping metals and the cooling conditions. Even though Ca and Mg are both alkaline-earth elements with similar chemical properties, Ca shows a higher affinity to the impurities. The reason is explained by the cation difference that Ca is larger, softer, and less polarizing compared to Mg, so that Ca exhibits a higher reactivity. It is also worth noting that the significant decline of purification efficiency by casting CM1-casted also highlights the critical role of cooling rate on impurity segregation that with a high cooling rate, impurities may undergo insufficient diffusion, finally, the segregation behavior is limited.

3.4. P removal modelling

The leaching results suggest that P segregation and its removal is strongly affected by Ca/Mg alloying ratio even though P is apt to segregate on Si grain boundary as well [60]. Thus, it is necessary to investigate the effect of Ca and Mg alloying on P segregation. In our previous work [16], a Gulliver-Scheil segregation based model for binary Si alloy system was developed to estimate the P removal degree after acid leaching combined with the thermodynamic properties of the doping metal. For an arbitrary Si-rich ternary alloying system Si-Me_1-Me_2, if the consideration is still limited to the dilute solution scheme, the model can be extended to the ternary system by ignoring the second-order interaction coefficient. Therefore, the P activity coefficient in the melt $\gamma_{P\ in\ Si-Me1-Me2(l)}$ can be written as the unified formalism proposed by Bale and Pelton [61]:

$$\ln \gamma_{P\ in\ Si-Me_1-Me_2(l)} = \ln\ \gamma_P^0 + \ln\ \gamma_{Si} + \varepsilon_P^P X_P + \varepsilon_{Me1}^P X_{Me1} + \varepsilon_{Me2}^P X_{Me2} \quad (7)$$

where γ_P^0 represents the activity coefficient of P in the solvent at infinite dilution, and γ_{Si} represents the activity coefficient of solvent Si, which is close to unity. ε_P^P, ε_{Me}^Prepresent the first order interaction coefficient of P itself and P with doping metal Me, and X_{Me} represents the concentration of doping metal Me in Si melt. However, the term ln γ_{Si} and $\varepsilon_P^P X_P$ can be ignored since they are close to zero. So that we have:

$$\frac{\gamma_{P\ in\ Si-Me_1-Me_2(l)}}{\gamma^0_{P\ in\ Si\ (l)}} = \exp\left(\varepsilon_{Me1}^P X_{Me1} + \varepsilon_{Me2}^P X_{Me2}\right) \quad (8)$$

Table 4
Impurity concentration of purified Si alloys and MG-Si.

Impurity	CM0.5	CM1	CM2	CM1-Casted	MG-Si
P	1.0	0.9	0.6	1.9	10.1
Ca	888.1	627.6	442.1	3865.7	59.1
Mg	1219.7	508.1	260.6	2781.4	2.3
Al	149.6	91.2	63.3	242.2	972.4
Fe	419.9	285.1	260.9	479.6	1470.9
Ti	37.7	26.4	24.4	46.9	129.8

It is known that at the equilibrium state, the chemical potential of P in the two phases are equal:

$$\mu_{in\ Si\ (s)} = \mu_{in\ Si-Me_1-Me_2\ (l)} \quad (9)$$

Subsequently, the following relationship is obtained in term of Gibbs energy and activities:

$$\Delta G^{\circ}_{P\ in\ Si\ (s)} + RTln\ a_{P\ in\ Si\ (s)} = \Delta G^{\circ}_{P\ in\ Si-Me_1-Me_2\ (l)} + \mathrm{RTln}a_{P\ in\ Si-Me_1-Me_2\ (l)} \quad (10)$$

After arrangement, and regarding the fact that Gibbs energy is a state function and there is only trace amount of P in the phases with insignificant Gibbs energies of dissolution (in solid and liquid phases), it yields:

$$\Delta G^{\circ fus}_{P\ in\ Si-Me_1-Me_2} = \Delta G^{\circ fus}_{P\ in\ Si} \quad (11)$$

$$\frac{a_{P\ in\ Si\ (s)}}{a_{P\ in\ Si-Me_1-Me_2(l)}} = \exp\left(\frac{\Delta G^{\circ fus}_{P\ in\ Si-Me_1-Me_2}}{RT}\right) \quad (12)$$

where $\Delta G^{\circ fus}_{P\ in\ Si}$and $\Delta G^{\circ fus}_{P\ in\ Si-Me1-Me2}$ indicate the Gibbs energy of fusion for P in Si and in the ternary system.

Moreover, the P segregation coefficient in the ternary system Si-Me_1-Me_2 can be expressed as:

$$k_P^{Si-Me1-Me2} = \frac{X_{P\ in\ Si(s)}}{X_{P\ in\ Si-Me_1-Me_2(l)}} = \exp\left(\frac{\Delta G^{\circ fus}_{P\ in\ Si-Me_1-Me_2}}{RT}\right)\frac{\gamma_{P\ in\ Si-Me_1-Me_2(l)}}{\gamma_{P\ in\ Si\ (s)}} \quad (13)$$

Similarly, for the binary Si-P system:

$$k_P^{Si} = \exp\left(\frac{\Delta G^{\circ fus}_{P\ in\ Si}}{RT}\right)\frac{\gamma^0_{P\ in\ Si\ (l)}}{\gamma^0_{P\ in\ Si\ (s)}} \quad (14)$$

Since the concentration of alloying elements in solid Si is neglectable, thus, $\gamma_{P\ in\ Si\ (s)} = \gamma^0_{P\ in\ Si\ (s)}$. Combining Eq. (8), Eq. (13), and Eq. (14):

$$k_P^{Si-Me1-Me2} = \exp\left(\frac{\Delta G^{\circ fus}_{P\ in\ Si}}{RT}\right)\frac{\gamma^0_{P\ in\ Si\ (l)}}{\gamma_{P\ in\ Si\ (s)}}\frac{\gamma_{P\ in\ Si-Me_1-Me_2(l)}}{\gamma^0_{P\ in\ Si\ (l)}} = k_P^{Si}\frac{\gamma_{P\ in\ Si-Me_1-Me_2(l)}}{\gamma^0_{P\ in\ Si\ (l)}} \quad (15)$$

By introducing Eq. (8), it then gives,

$$k_P^{Si-Me1-Me2} = k_P^{Si}\exp\left(\varepsilon_{Me1}^P X_{Me1} + \varepsilon_{Me2}^P X_{Me2}\right) \quad (16)$$

It is assumed that all doping metals will stay in the remaining liquid phase during solidification due to their very low segregation coefficients, thus, Eq.(17) can be obtained for when a fraction f_s is solidified:

$$X_{Me} = \frac{X_{Me}^{initial}}{(1-f_s)} \quad (17)$$

And,

$$k_P^{Si-Me1-Me2} = k_P^{Si}\exp\left(\frac{\varepsilon_{Me1}^P X_{Me1} + \varepsilon_{Me2}^P X_{Me2}}{1-f_s}\right) \quad (18)$$

The P removal degree is defined as the ratio of the removed P over the initial P in Si before doping, which is written as:

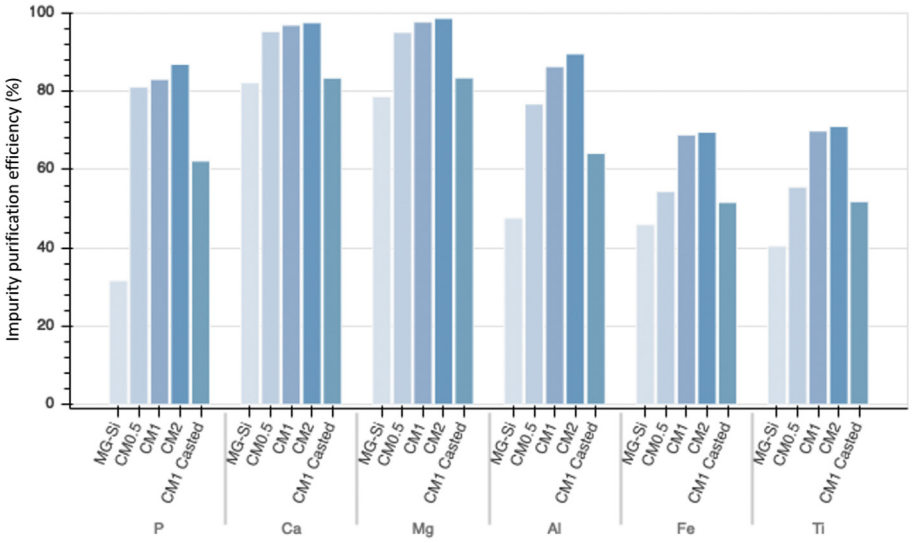

Fig. 8. Purification efficiency of studied Si-Ca-Mg alloys and MG-Si leached by HCl at 60 °C for 3 h, particle size: 0.2–1 mm. (digital version in color).

$$\eta = \left(\frac{X^{initial}_{\mathrm{P\ in\ Si}(l)} - X_{\mathrm{P\ in\ Si(s)}}}{X^{initial}_{\mathrm{P\ in\ Si}(l)}}\right) \times 100\% \quad (19)$$

where $X^{initial}_{\mathrm{P\ in\ Si}(l)}$ and $\overline{X}_{\mathrm{P\ in\ Si(s)}}$ represent the initial P concentration in Si and the averaged P concentration in purified Si after leaching.

Herein, $\overline{X}_{\mathrm{P\ in\ Si(s)}}$ can be obtained by integrating the Gulliver-Scheil equation from the starting point of solidification to the eutectic point:

$$X_{\mathrm{P\ in\ Si(s)}} = \frac{X^{initial}_{\mathrm{P\ in\ Si}(l)}}{f^{Eu}_s}\left(1-\left(1-f^{Eu}_s\right)^{k_P^{\mathrm{Si-Me1-Me2}}}\right) \quad (20)$$

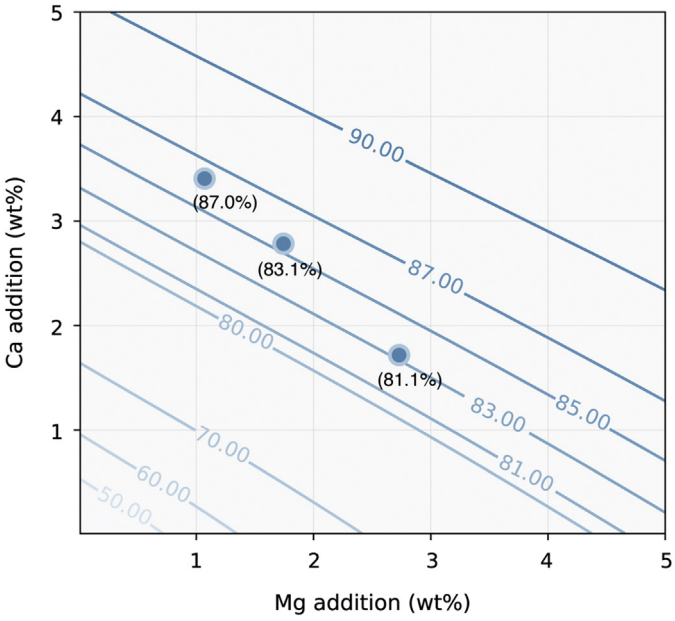

Fig. 9. Comparison between predicted (solid lines) and measured (scatters with numbers in parentheses) P removal degree of Si-Ca-Mg alloying-leaching system. (digital version in color).

With,

$$X^{Eu}_{\mathrm{P\ in\ Si}\ (l)} = X^{initial}_{\mathrm{P\ in\ Si}(l)}\left(f^{Eu}_s\right)^{k_P^{\mathrm{Si-Me1-Me2}}-1} \quad (21)$$

Thus, after rearrangement, the P removal degree can be further rewritten as:

$$\eta = \left(1-\frac{1-\frac{X^{\mathrm{P\ in\ Si}\ (l)}}{X^{initial}_{\mathrm{P\ in\ Si}(l)}}\left(1-f^{Eu}_s\right)}{f^{Eu}_s}\right) \times 100\% \quad (22)$$

To further cope with the expression of the $\frac{X^{Eu}_{\mathrm{P\ in\ Si}\ (l)}}{X^{initial}_{\mathrm{P\ in\ Si}(l)}}$, the definition of Gulliver-Scheil equation:

$$(1-f_s)\mathrm{d}X_{\mathrm{P}(l)} = (X_{\mathrm{P}(l)} - X_{\mathrm{P}(s)})\mathrm{d}f_s \quad (23)$$

Considering the relationship $X_{\mathrm{P}(s)} = k_P^{\mathrm{Si-Me1-Me2}}X_{\mathrm{P}(l)}$, it yields:

$$\frac{\mathrm{d}X_{\mathrm{P}(l)}}{X_{\mathrm{P}(l)}} = \frac{1-k_P^{\mathrm{Si-Me1-Me2}}}{(1-f_s)}\mathrm{d}f_s \quad (24)$$

The term is thus obtained after integration:

$$\ln\frac{X^{Eu}_{\mathrm{P\ in\ Si}(l)}}{X^{initial}_{\mathrm{P\ in\ Si}(l)}} = \int_0^{f^{Eu}_s}\frac{1-k_P^{\mathrm{Si-Me1-Me2}}}{1-f_s}\mathrm{d}f_s \quad (25)$$

Finally, the P removal degree model for ternary alloy system is obtained:

$$\eta = \left(1-\frac{1-\frac{\exp\left(k_P^{Si}E_i\left(\frac{\varepsilon^P_{Me1}X_{Me1}+\varepsilon^P_{Me2}X_{Me2}}{1-f^{Eu}_s}\right)\right)}{\exp\left(k_P^{Si}E_i\left(\varepsilon^P_{Me1}X_{Me1}+\varepsilon^P_{Me2}X_{Me2}\right)\right)}}{f^{Eu}_s}\right) \quad (26)$$

where the $E_i(x)$ function represents the exponential integral $E_i(x) = \int_{-\infty}^{x}\frac{e^t dt}{t}$.

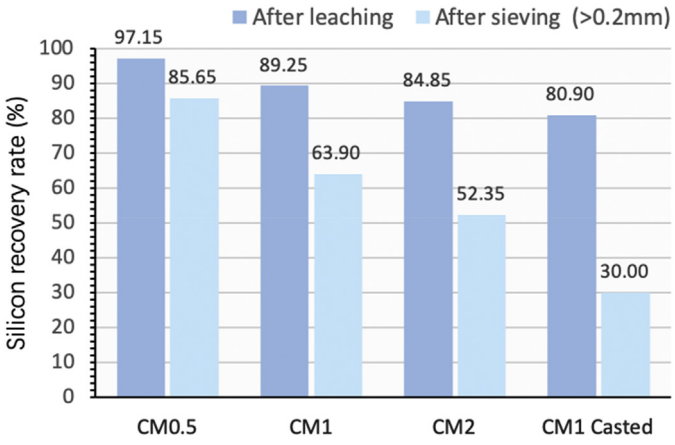

Fig. 10. Si recovery rates for particle size 0.2–1 mm. The dark blue column (left) indicates the Si recovery rate measured by the weight ratio of all obtained materials and charged materials; the light blue column (right) indicates the weight ratio of particle size bigger than 0.2 mm and charged materials. (digital version in color).

Subsequently, for the Si-Ca-Mg alloying system, we have:

$$\eta = \left(1 - \frac{1 - \frac{\exp\left(k_P^{Si} E_i \left(\frac{\varepsilon_{Ca}^P X_{Ca\ in\ Si(l)}^{initial} + \varepsilon_{Mg}^P X_{Mg\ in\ Si(l)}^{initial}}{1 - f_s^{Eu}}\right)\right)}{\exp\left(k_P^{Si} E_i \left(\varepsilon_{Ca}^P X_{Ca\ in\ Si(l)}^{initial} + \varepsilon_{Mg}^P X_{Mg\ in\ Si(l)}^{initial}\right)\right)}}{f_s^{Eu}}\right) \quad (27)$$

The results of measured and predicted P removal degree after acid leaching are presented in Fig. 9. Good agreement can be seen by using the previously obtained value $\varepsilon_{Mg}^P = -10.8$ for Mg-P interaction [16] and the estimated value $\varepsilon_{Ca}^P = -22.4$ is calculated from the Waseda model [62] at 1687 K. Since ε_{Ca}^P is more negative, it is seen that with fixed P removal degree, less metal doping amount is needed for Ca. Furthermore, the model also suggests an essential parameter for the alloying-leaching process that 80% P removal can be reached by alloying around 4.5 wt% Mg or 3 wt% Ca, while for the Si-Ca-Mg ternary alloying-leaching, between 3 and 4.5 wt% metal alloying is needed.

3.5. Si recovery

Si recovery rate is a critical index which directly determines the process profits and feasibility. However, the effect of alloying composition and solidification conditions on the Si recovery is still rarely reported. By measuring the weight of material before and after leaching, the results of Si recovery rate of the studied Si-Ca-Mg alloys are shown in Fig. 10. It is apparently seen that Si recovery follows the order: CM0.5 (97.15%) > CM1 (89.25%) > CM2 (84.85%) > CM1-Casted (80.90%). The reason is attributed to the increasing particle disintegration with increasing Ca/Mg ratio that enhanced the fine particle loss in the post-cleaning and washing process. A more distinct trend can be seen by sieving out fine particles with a diameter of less than 0.2 mm (the minimum charging particle size) that the Si recovery significantly decreases with increasing Ca/Mg ratio and by casting. For example, only 52.35% and 30.00% Si were recovered for sample CM2 and CM1-Casted. Thus, even though a high Ca/Mg mixing ratio brings a better leaching efficiency, but it is, however, detrimental to the Si recovery. This result suggests that an optimal alloy composition design should balance the impurity removal efficiency and the final Si yield. Additionally, by comparing CM1 and CM1-Casted, cooling rate also plays an important role on Si recovery as the finer Si grain resulted by fast cooling (as presented in Fig. 4) may lead to higher Si loss in the purification process.

4. Conclusions

In the present work, a parametric study was carried on studying the effect of Ca/Mg mixing ratio and solidification conditions on the Si alloying-leaching purification. The results can be summarized as follows:

(1) $Ca_7Mg_{7.5\pm6}Si_{14}$ was found as the main phase of all studied Si-Ca-Mg alloys that gathering impurities and affect leaching behavior, while Mg_2Si and $CaSi_2$ appear depends on the Ca/Mg mixing ratio. Compared to furnace cooling, rapid cooling reduces Si grain size distinctly and suppresses impurity segregation.
(2) HCl is found as the most economical leaching agents among the studied combinations. Finer particle size promotes higher leaching efficiency, but with increasing Ca/Mg ratio, the increment narrows.
(3) The leaching kinetics of Si-Ca-Mg alloys follows a cracking-shrinking model on the basis of the modification of Kröger-Ziegler model under spherical condition.
(4) Impurity purification efficiency increases with increasing Ca/Mg mixing ratio but considerably decreases with fast cooling.
(5) A model for P removal degree prediction was developed for ternary alloy system and in good agreement with the leaching results of the studied Si-Ca-Mg alloys.

Declaration of Competing Interest

The authors declare that they have no known competing financial interests or personal relationships that could have appeared to influence the work reported in this paper.

Acknowledgment

This work was performed at NTNU within the Research Centre for Sustainable Solar Cell Technology (FME SuSolTech, project number 257639), co-sponsored by the Norwegian Research Council and industry partners. The authors also appreciate the fruitful discussions with Arman Hoseinpur and the ICP-MS assistance by Gagan Paudel from NTNU.

References

[1] A. Murgau, J. Safarian, Solar silicon production through metallurgical route and REC solar advancements, Silicon Chem. Sol. Ind. XIV (2018) 183–192 Svolvær, Norway.
[2] J. Safarian, M. Tangstad, Processes for upgrading metallurgical grade silicon to solar grade silicon, Energy Procedia 20 (2012) 88–97, https://doi.org/10.1016/J.EGYPRO.2012.03.011.
[3] Z. Yu, W. Ma, K. Xie, G. Lv, Z. Chen, J. Wu, J. Yu, Life cycle assessment of grid-connected power generation from metallurgical route multi-crystalline silicon photovoltaic system in China, Appl. Energy 185 (2017) 68–81, https://doi.org/10.1016/j.apenergy.2016.10.051.
[4] J. Safarian, G. Tranell, M. Tangstad, Boron removal from silicon by CaO-Na2O-SiO2 ternary slag, Metall. Mater. Trans. E. 2 (2015) 109–118, https://doi.org/10.1007/s40553-015-0048-7.
[5] L.A.V. Teixeira, K. Morita, Removal of boron from molten silicon using CaO-SiO2 based slags, ISIJ Int. 49 (2009) 783–787, https://doi.org/10.2355/isijinternational.49.783.
[6] J. Wu, D. Yang, M. Xu, W. Ma, Q. Zhou, Z. Xia, Y. Lei, K. Wei, S. Li, Z. Chen, K. Xie, Boron removal from silicon using secondary refining techniques by metallurgical method, Sep. Purif. Rev. 49 (2020) 68–88, https://doi.org/10.1080/15422119.2018.1523191.
[7] Y. Wang, K. Morita, Evaporation removal of boron in molten silicon using reactive fluxes, Miner. Met. Mater. Ser. (2017) 367–375, https://doi.org/10.1007/978-3-319-52192-3_36.
[8] M. Fang, C. Lu, L. Huang, H. Lai, J. Chen, X. Yang, J. Li, W. Ma, P. Xing, X. Luo, Multiple slag operation on boron removal from metallurgical-grade silicon using Na2O-SiO2 slags, Ind. Eng. Chem. Res. 53 (2014) 12054–12062, https://doi.org/10.1021/ie404427c.

[9] J. Wu, F. Wang, W. Ma, Y. Lei, B. Yang, Thermodynamics and kinetics of boron removal from metallurgical grade silicon by addition of high basic potassium carbonate to calcium silicate slag, Metall. Mater. Trans. B Process Metall. Mater. Process. Sci. 47 (2016) 1796–1803, https://doi.org/10.1007/s11663-016-0615-z.

[10] H. Chen, K. Morita, X. Ma, Z. Chen, Y. Wang, Boron removal for solar-grade silicon production by metallurgical route:a review, Sol. Energy Mater. Sol. Cells 203 (2019) 110169, https://doi.org/10.1016/j.solmat.2019.110169.

[11] T. Yoshikawa, K. Morita, Refining of silicon during its solidification from a Si–Al melt, J. Cryst. Growth 311 (2009) 776–779, https://doi.org/10.1016/J.JCRYSGRO.2008.09.095.

[12] L. Huang, H. Lai, C. Lu, M. Fang, W. Ma, P. Xing, J. Li, X. Luo, Enhancement in extraction of boron and phosphorus from metallurgical grade silicon by copper alloying and aqua regia leaching, Hydrometallurgy. 161 (2016) 14–21, https://doi.org/10.1016/j.hydromet.2016.01.013.

[13] L.T. Khajavi, K. Morita, T. Yoshikawa, M. Barati, Removal of boron from silicon by solvent refining using ferrosilicon alloys, Metall. Mater. Trans. B Process Metall. Mater. Process. Sci. 46 (2014) 615–620, https://doi.org/10.1007/s11663-014-0236-3.

[14] X. Ma, T. Yoshikawa, K. Morita, Si growth by directional solidification of Si–Sn alloys to produce solar-grade Si, J. Cryst. Growth 377 (2013) 192–196, https://doi.org/10.1016/J.JCRYSGRO.2013.05.024.

[15] Y. Li, L. Zhang, Application of Si-based solvents to the purification of metallurgical grade-silicon, Sep. Purif. Rev. (2019) 1–24, https://doi.org/10.1080/15422119.2019.1623253.

[16] M. Zhu, A. Azarov, E. Monakhov, K. Tang, J. Safarian, Phosphorus separation from metallurgical-grade silicon by magnesium alloying and acid leaching, Sep. Purif. Technol. 240 (2020) 116614, https://doi.org/10.1016/j.seppur.2020.116614.

[17] A. Schei, Metallurgical production of high purity silicon, 4th Int.Ferro Alloys Cong. (1986) 389–398 Rio de Janeiro, Brazil.

[18] H. Lai, L. Huang, C. Lu, M. Fang, W. Ma, P. Xing, J. Li, X. Luo, Leaching behavior of impurities in Ca-alloyed metallurgical grade silicon, Hydrometallurgy. 156 (2015) 173–181, https://doi.org/10.1016/j.hydromet.2015.06.012.

[19] J. Safarian, M. Tangstad, Vacuum refining of molten silicon, Metall. Mater. Trans. B Process Metall. Mater. Process. Sci. 43 (2012) 1427–1445, https://doi.org/10.1007/s11663-012-9728-1.

[20] A. Hoseinpur, K. Tang, J. Safarian, Kinetic study of vacuum evaporation of elements from ternary melts; case of dilute solution of P in Si-Al melts, Sep. Purif. Technol. 235 (2020)https://doi.org/10.1016/j.seppur.2019.116284.

[21] S.-S. Zheng, T. Abel Engh, M. Tangstad, X.-T. Luo, Separation of phosphorus from silicon by induction vacuum refining, Sep. Purif. Technol. 82 (2011) 128–137, https://doi.org/10.1016/j.seppur.2011.09.001.

[22] J. Safarian, K. Tang, K. Hildal, G. Tranell, Boron removal from silicon by humidified gases, Metall. Mater. Trans. E. 1 (2014) 41–47, https://doi.org/10.1007/s40553-014-0007-8.

[23] Ø.S. Sortland, M. Tangstad, Boron removal from silicon melts by H2O/H2 gas blowing: mass transfer in gas and melt, Metall. Mater. Trans. E. 1 (2014) 211–225, https://doi.org/10.1007/s40553-014-0021-x.

[24] Z. Xia, J. Wu, W. Ma, Y. Lei, K. Wei, Y. Dai, Separation of boron from metallurgical grade silicon by a synthetic CaO-CaCl2 slag treatment and Ar-H2O-O2 gas blowing refining technique, Sep. Purif. Technol. 187 (2017) 25–33, https://doi.org/10.1016/j.seppur.2017.06.037.

[25] J. Wu, Y. Zhou, W. Ma, M. Xu, B. Yang, Synergistic separation behavior of boron in metallurgical grade silicon using a combined slagging and gas blowing refining technique, Metall. Mater. Trans. B Process Metall. Mater. Process. Sci. 48 (2017) 22–26, https://doi.org/10.1007/s11663-016-0860-1.

[26] N.P. Tucker, Preparation of high purity silicon, J. Iron Steel Ind. 15 (1927) 412–414.

[27] L.P. Hunt, V.D. Dosaj, J.R. McCormick, L.D. Crossman, Production of solar-grade silicon from purified metallurgical silicon, 12th IEEE Photovolt. Spec. Conf. (1976) 125–129.

[28] J. Dietl, Hydrometallurgical purification of metallurgical-grade silicon, Sol. Cells. 10 (1983) 145–154, https://doi.org/10.1016/0379-6787(83)90015-7.

[29] I.C. Santos, A.P. Goncalves, C.S. Santos, M. Almeida, M.H. Afonso, M.J. Cruz, Purification of metallurgical grade silicon by acid leaching, Hydrometallurgy. 23 (1990) 237–246, https://doi.org/10.4028/www.scientific.net/AMR.418-420.1590.

[30] T.L. Chu, S.S. Chu, Partial purification of metallurgical silicon by acid extraction, J. Electrochem. Soc. 130 (1983) 455, https://doi.org/10.1149/1.2119730.

[31] H. Lu, K. Wei, W. Ma, K. Xie, J. Wu, Y. Lei, The effect of secondary refining on the removal of phosphorus from metallurgical-grade silicon by acid leaching, Metall. Mater. Trans. B Process Metall. Mater. Process. Sci. 48 (2017) 2768–2780, https://doi.org/10.1007/s11663-017-1042-5.

[32] E. Kim, K. Osseo-Asare, Dissolution windows for hydrometallurgical purification of metallurgical-grade silicon to solar-grade silicon: eh–pH diagrams for Fe silicides, Hydrometallurgy. 127–128 (2012) 178–186, https://doi.org/10.1016/J.HYDROMET.2012.05.013.

[33] F. Margarido, J.P. Martins, M.O. Figueiredo, M.H. Bastos, Kinetics of acid leaching refining of an industrial Fe-Si alloy, Hydrometallurgy. 34 (1993) 1–11, https://doi.org/10.1016/0304-386X(93)90077-Q.

[34] F. Margarido, M.H. Bastos, M.O. Figueiredo, J.P. Martins, The structural effect on the kinetics of acid leaching refining of Fe-Si alloys, Mater. Chem. Phys. 38 (1994) 342–347, https://doi.org/10.1016/0254-0584(94)90211-9.

[35] J.P. Martins, F. Margarido, The cracking shrinking model for solid-fluid reactions, Mater. Chem. Phys. 44 (1996) 156–169, https://doi.org/10.1016/0254-0584(95)01670-P.

[36] T. Yoshikawa, K. Morita, An evolving method for solar-grade silicon production: solvent refining, Jom. 64 (2012) 946–951, https://doi.org/10.1007/s11837-012-0371-8.

[37] B. Ban, X. Bai, J. Li, J. Chen, S. Dai, Effect of kinetics on P removal by Al-Si solvent refining at low solidification temperature, J. Alloys Compd. 685 (2016) 604–609, https://doi.org/10.1016/j.jallcom.2016.05.312.

[38] J. Li, Y. Liu, Y. Tan, Y. Li, L. Zhang, S. Wu, P. Jia, Effect of tin addition on primary silicon recovery in Si–Al melt during solidification refining of silicon, J. Cryst. Growth 371 (2013) 1–6, https://doi.org/10.1016/J.JCRYSGRO.2012.12.098.

[39] G. Qian, L. Sun, H. Chen, Z. Wang, K. Wei, W. Ma, Enhancing impurities removal from Si by controlling crystal growth in directional solidification refining with Al–Si alloy, J. Alloys Compd. 820 (2020) 153300, https://doi.org/10.1016/j.jallcom.2019.153300.

[40] Y. Li, Y. Tan, J. Li, K. Morita, Si purity control and separation from Si–Al alloy melt with Zn addition, J. Alloys Compd. 611 (2014) 267–272, https://doi.org/10.1016/J.JALLCOM.2014.05.138.

[41] Y. Lei, P. Qiu, K. Chen, X. Chen, W. Ma, J. Wu, K. Wei, S. Li, G. Lv, J. Qiu, Mechanism of ZrB2 formation in Al-Si alloy and application in Si purification, ACS Sustain. Chem. Eng. 7 (2019) 12990–12996, https://doi.org/10.1021/acssuschemeng.9b02065.

[42] L. Huang, J. Chen, A. Danaei, S. Thomas, L. Huang, X. Luo, M. Barati, Effect of Ti addition to cu-Si alloy on the boron distribution in various phases, J. Alloys Compd. 734 (2018) 235–242, https://doi.org/10.1016/j.jallcom.2017.10.279.

[43] L. Tafaghodi Khajavi, M. Barati, Thermodynamics of phosphorus in solvent refining of silicon using ferrosilicon alloys, Metall. Mater. Trans. B Process Metall. Mater. Process. Sci. 48 (2017) 268–275, https://doi.org/10.1007/s11663-016-0804-9.

[44] L.T. Khajavi, K. Morita, T. Yoshikawa, M. Barati, Thermodynamics of boron distribution in solvent refining of silicon using ferrosilicon alloys, J. Alloys Compd. 619 (2015) 634–638, https://doi.org/10.1016/j.jallcom.2014.09.062.

[45] F. Yang, J. Wu, W. Ma, Thermodynamic modeling and experimental study on interaction of Fe to P in silicon solution, Metall. Mater. Trans. B Process Metall. Mater. Process. Sci. 51 (2020) 2381–2390, https://doi.org/10.1007/s11663-020-01895-9.

[46] T. Shimpo, T. Yoshikawa, K. Morita, Thermodynamic study of the effect of calcium on removal of phosphorus from silicon by acid leaching treatment, Metall. Mater. Trans. B Process Metall. Mater. Process. Sci. 35 (2004) 277–284, https://doi.org/10.1007/s11663-004-0029-1.

[47] Y.V. Meteleva-Fischer, Y. Yang, R. Boom, B. Kraaijveld, H. Kuntzel, Microstructure of metallurgical grade silicon and its acid leaching behaviour by alloying with calcium, Trans. Institutions Min. Metall. Sect. C Miner. Process. Extr. Metall. 122 (2013) 229–237, https://doi.org/10.1179/0371955313Z.00000000068.

[48] M.D. Johnston, M. Barati, Calcium and titanium as impurity getter metals in purification of silicon, Sep. Purif. Technol. 107 (2013) 129–134, https://doi.org/10.1016/j.seppur.2013.01.028.

[49] H. Sakiani, S.H. Tabaian, J. Chen, Effect of calcium addition on the silicon purification in the presence of low concentration of iron, J. Alloys Compd. 830 (2020) 154112, https://doi.org/10.1016/j.jallcom.2020.154112.

[50] J. Safarian, S. Espelien, Hydrometallurgical purification of Maganesium-doped silicon by difference acids, 33 Eur. Photovolt. Sol. Energy Conf. Exhib. (2017) 480–482.

[51] M. Zhu, A. Murgau, J. Safarian, Effects of magnesium-doping on silicon leaching for solar grade feedstock production, 35 Eur. Photovolt. Sol. Energy Conf. Exhib. (2018) 465–468, https://doi.org/10.4229/35thEUPVSEC20182018-2AV.1.3.

[52] M. Zhu, S.Y. Yue, K. Tang, J. Safarian, New insights into silicon purification by alloying—leaching refining: a comparative study of Mg—Si, Ca—Si, and Ca—Mg—Si systems, ACS Sustain. Chem. Eng. 8 (42) (2020) 15953–15966, https://doi.org/10.1021/acssuschemeng.0c05564.

[53] S. Espelien, G. Tranell, J. Safarian, Effect of magnesium addition on removal of impurities from silicon by hydrometallurgical treatment, in: Energy Technol. 2017, Springer, 2017: pp. 355–366. doi: https://doi.org/10.1007/978-3-319-52192-3_35.

[54] S. Cui, M. Paliwal, I.-H. Jung, Thermodynamic Optimization of Ca-Fe-Si System and Its Applications to Metallurgical Grade Si-Refining Process, 2020https://doi.org/10.1007/s40553-014-0010-0.

[55] M.C.J. Marker, B. Skolyszewska-Kühberger, H.S. Effenberger, C. Schmetterer, K.W. Richter, Phase equilibria and structural investigations in the system Al-Fe-Si, Intermetallics. 19 (2011) 1919–1929, https://doi.org/10.1016/j.intermet.2011.05.003.

[56] Y.V. Meteleva-Fischer, Y. Yang, R. Boom, B. Kraaijveld, H. Kuntzel, Microstructure of metallurgical grade silicon during alloying refining with calcium, Intermetallics. 25 (2012) 9–17, https://doi.org/10.1016/j.intermet.2012.02.009.

[57] B. Ban, X. Bai, J. Li, Y. Li, J. Chen, S. Dai, The mechanism of P removal by solvent refining in Al-Si-P system, Metall. Mater. Trans. B Process Metall. Mater. Process. Sci. 46 (2015) 2430–2437, https://doi.org/10.1007/s11663-015-0449-0.

[58] E. Kim, K. Osseo-Asare, Dissolution windows for hydrometallurgical purification of metallurgical-grade silicon to solar-grade silicon: eh-pH diagrams for Fe silicides, Hydrometallurgy. 127–128 (2012) 178–186, https://doi.org/10.1016/j.hydromet.2012.05.013.

[59] J.P. Martins, F. Margarido, The cracking shrinking model for solid-fluid reactions, Mater. Chem. Phys. 44 (1996) 156–169, https://doi.org/10.1016/0254-0584(95)01670-P.

[60] D. Zhao, Y. Li, Revealing the factors influencing grain boundary segregation of P, as in Si: insights from first-principles, Acta Mater. 168 (2019) 52–62, https://doi.org/10.1016/J.ACTAMAT.2019.02.014.

[61] C.W. Bale, A.D. Pelton, The unified interaction parameter formalism: thermodynamic consistency and applications, Metall. Mater. Trans. A 21A (1989).

[62] S. Ueno, Y. Waseda, K.T. Jacob, S. Tamaki, Theoretical treatment of interaction parameters in multicomponent metallic solutions, Steel Res. 59 (1988).